PROCEEDINGS OF SCIENCE

Performance highlights in ATLAS

Antonio Giannini[a,*] **on behalf of the ATLAS Collaboration**

[a] *University of Science and Technology of China,*
No.96, JinZhai Road Baohe District, Hefei, Anhui, 230026, P.R.China

E-mail: antonio.giannini@cern.ch

The Run-2 data taking period of the LHC ended in 2018 and Run-3 is currently ongoing. While the new data are being recorded, the precision results and new methods have been applied in the reconstruction workflows in ATLAS. In this review a walk-through of recent achievements for each of the objects is taken, tracking, muons, electrons/photons, jets/missing transverse momentum, flavor and jet tagging, and hadronically decaying τ-leptons will be discussed in this order. The highlights will be on updated results for Run-2, which in most cases form the basis for Run-3 reconstruction, including new techniques that will be used in Run-3 or in the future.

ATL-PHYS-PROC-2024-102
30 October 2024

12th Large Hadron Collider Physics Conference (LHCP2024)
3-7 June 2024
Boston, USA

*Speaker

1. Introduction

The reconstruction of physical objects is based on the input of each subdetector of ATLAS [1]. The Physics program at the LHC [2] is very broad, and the reconstruction can play a crucial role in Standard Model (SM) measurements or to perform new searches for Beyond the Standard Model (BSM) physics.

2. Tracking

The Inner Detector (ID) is the subdetector closest to the interaction point and provides input to the reconstruction of all other objects. Charged particle reconstruction is a challenging task for the reconstruction software due to the combinatorial complexity and the software has been adapted to work more efficiently [3]. Updated track reconstruction is made faster by a factor two without a significant reduction in reconstruction efficiency as shown in Figure 1(a). Large Radius Tracking (LRT) reconstruction is now included for all events with an improvement in CPU requirements. LRT reconstruction allows to recover signal efficiency for searches of long-lived particles, light mass Higgs bosons and heavy neutral lepton models [4].

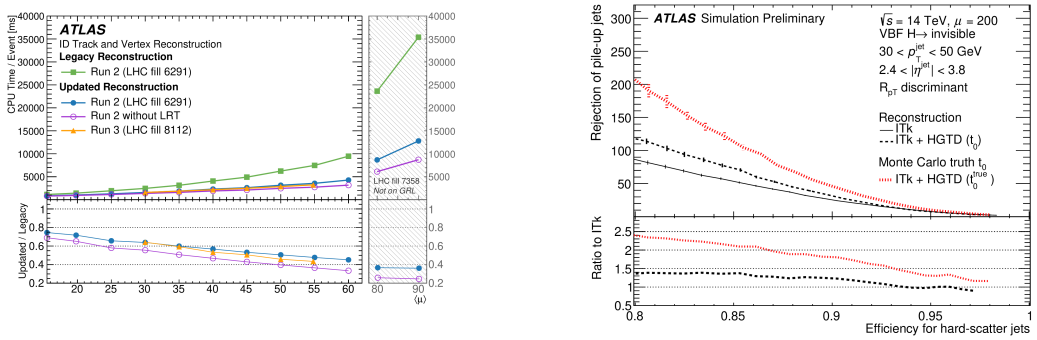

(a) (b)

Figure 1: (a) Processing time taken per event versus average pile-up to reconstruct ID tracks and vertices in the same events, for the the updated (purple) and legacy (green) reconstruction software; the updated reconstruction is also evaluated when including the impact of the additional LRT step (blue) [3]. (b) Impact of track time information on VBF Higgs boson production; the rejection of pile-up jets as a function of the efficiency for hard-scatter jets with an average of 200 pile-up collisions per bunch crossing [5].

A new Machine Learning (ML)-based technique for primary vertex (PV) reconstruction has been studied, which achieves better efficiency than the baseline algorithm [6]. Tracking reconstruction is directly affected by the new detectors planned for the HL-LHC [7]. The reconstruction efficiency after introducing a full-silicon Inner Tracker (ITk) detector [8] has been studied with simulations. When compared with Run-3 conditions, the efficiency results are comparable in the overlapping geometrical region ($|\eta| < 2.4$) while an extra coverage above, up to $|\eta| < 4$. will provide efficiencies of 80-90%. The performance improvement in the forward region has been tested also adding the High-Granularity Timing Detector (HGTD) detector [5]. Improvements are expected in several use cases, the gain in the invisible Vector Boson Fusion (VBF) Higgs boson ($h \to \nu\nu$) analysis is shown in Figure 1(b).

3. Muons

Muon reconstruction is based on tracks, combining the ID and Muon Spectrometer (MS) subdetectors, and on inputs from the calorimeters. High precision calibration results are obtained with Run-2 data [9] and the di-muon invariant mass is shown in Figure 2(a). The momentum resolution and the interplay between the ID and MS are shown in Figure 2(b). Z and J/ψ events are used and the calibration is then validated on Υ events. The accuracy is reduced to 0.05% and the resolution to 1.5%. Finally, a novel approach is used to correct the charge bias for calibration up to 450 GeV and 0.03/TeV accuracy.

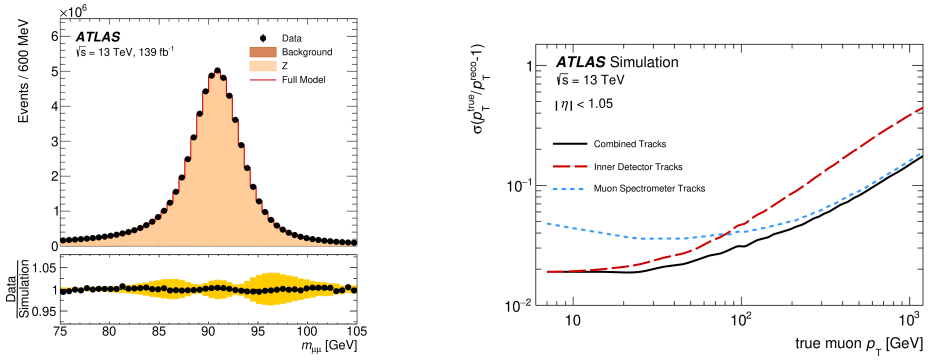

(a) (b)

Figure 2: (a) Resolution of the muon p_{T} obtained from simulation as a function of the true p_{T} of the muon for a range up to η=1 [9]. (b) Di-muon invariant mass distribution of $Z \to \mu\mu$ events [9].

4. Electrons and photons

The reconstruction of electrons and photons is closely related and relies on the combination of tracking and calorimetric information. Prompt energy deposits in the calorimeters are discriminated from secondary deposits and other electromagnetic activity. The absolute energy scale is set using a large sample of Z boson decaying in electron-positron pairs [10], and its residual dependence on electron energy is first used to further constrain systematic uncertainties. The impact of uncertainties on the energy scale is shown in Figure 3(a). For electron identification (ID) three Working Points (WPs) are defined [11]. Large background rejection factors are achieved. For background from heavy-flavor decays, in general, the discrimination is lower as shown in Figure 3(b). A significant improvement in the ID efficiency uncertainties has been achieved, for electrons they are better compared to Run-1 at 8 TeV and above 40 GeV even compared to 7 TeV data taking period, despite different pile-up (PU) conditions. ID for photons has been also updated using the combination of three different methods. Different WPs were defined for electron and photon isolation, they usually account for different needs of analysis exploting final states with electrons and/or photons.

5. Missing E_{T}, jets calibration and tagging

The neutrino momentum can not be directly reconstructed as these particles do not interact with the detector. The missing transverse energy, $E_{\mathrm{T}}^{\mathrm{miss}}$, is instead reconstructed as the missing

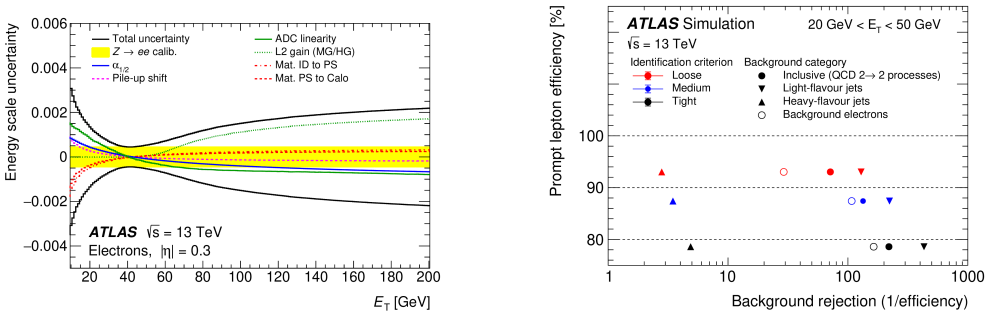

(a) (b)

Figure 3: (a) Relative energy scale calibration uncertainty for electrons as a function of E_T for $|\eta| = 0.3$ [10]. (b) The identification efficiency of signal electrons as a function of the background rejection [11].

component after imposing the energy conservation in the transverse plane. New Run-2 results report improvements on the E_T^{miss} scale and resolution [12]. Clusters of topologically connected calorimeter cells with significant energy deposit and large absolute signal-to-noise ratio (topo clusters) are the basis of the calorimeter reconstruction. Topo clusters reconstruction is improved by adding a calorimeter-cell timing criterion to the signal to noise ratio requirement in the clustering algorithm [13]. The new criterion allows to reduce the out of time PU up to 50% on the jet multiplicity at 20 GeV and up to 80% for above 50 GeV and it is included in Run-3 reconstruction. A new Global Neural Network Calibration (GNNC) procedure is applied for small-R (jet radius R=0.4) jets calibration [14]. This allows better exploitation of all input variables and better p_T scale and resolution as shown in Figure 4(a). In-situ p_T calibration up to 1% accuracy are obtained. For large-R (R=1.0) jets, a simultaneous calibration of p_T and mass is performed [15], obtaining a resolution better than in the baseline procedures as shown in Figure 4(b). A jet originated from

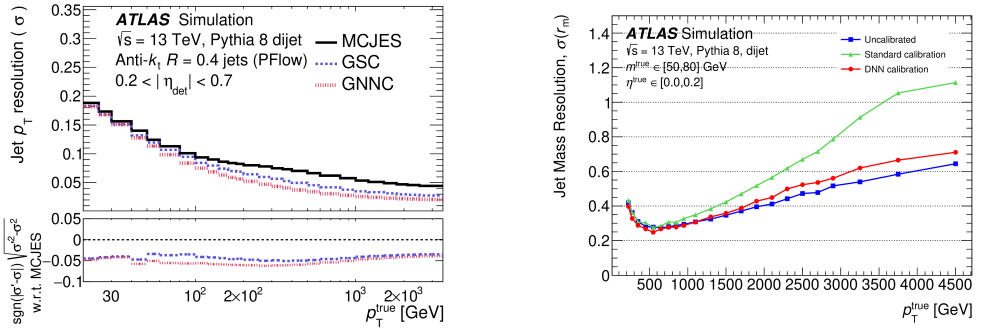

(a) (b)

Figure 4: (a) The jet p_T resolution for $0.2 < |\eta| < 0.7$; the solid line shows the MCJES, the long dashed line shows the Global Sequential Calibration (GSC), and the short dashed line shows the GNNC [14]. (b) Jet mass resolutions for different calibrations (squares: no calibration, triangles: standard calibration, circles: Deep Neural Network (DNN) calibration) as a function of true p_T [15].

a heavy flavor quark or from the hadronic decay of a W/Z or h boson can be discriminated from

jets initiated from a gluon or a light quark (jet tagging). A technique based on analysing tracks using a Graph Neural Network (GNN) is replacing the low-level optimized discriminants chain [16]. Tagging of boosted objects is interesting for high-mass searches and SM measurements in

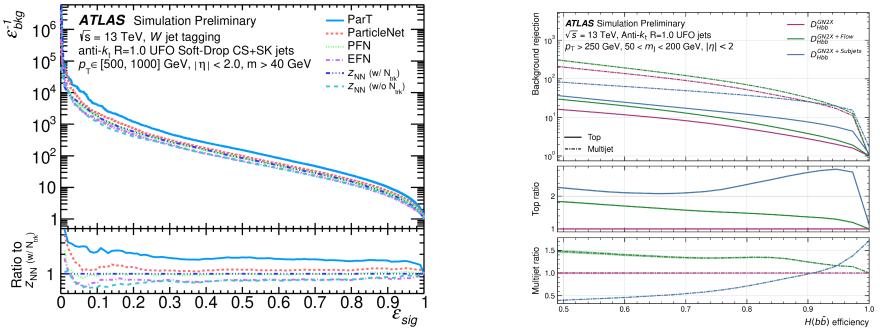

(a) (b)

Figure 5: (a) The QCD jets background rejection versus the W jets signal efficiency; all of the constituent-based taggers studied surpass the performance of the high-level-feature-based tagger (zNN) [17]. (b) The top and multijet background rejection as a function of the $h \to b\bar{b}$ tagging efficiency [18].

boosted regimes. Several approaches are designed to capture the two-prong nature of W/Z bosons [17] as shown in Figure 5(a), three-prong for the top or two-prong with heavy flavor for h boson decay [18] as shown in Figure 5(b).

6. Hadronically decaying τ-leptons (τ_{had})

For hadronically decaying τ-leptons (τ_{had}), ML is used through some parts of the τ_{had} reconstruction [19]. The reconstruction and ID are based on Recurrent Neural Network (RNN) as shown in Figure 6(a). The decay mode classification is based on a DeepSet which allows for better computational performance with respect to RNN models. The p_{T} resolution is improved by performing a regression based on the detector information that allows to reach order of 5% with a dedicated Boosted Regression Tree (BRT) calibration as shown in Figure 6(b).

7. Conclusions

The final performance results for Run-2 have been summarised. Improved techniques and results are achieved and they will also be used during Run-3. Run-3 is in ongoing as well as the reconstruction work of the new data for muons [20], for electrons/photons [21], for flavor tagging [22]; they are the basis for new exciting results in the future.

References

[1] ATLAS Collaboration, *JINST* **3** (2008) S08003.

[2] L. Evans and P. Bryant, *JINST* **3** (2008) S08001.

[3] ATLAS Collaboration, *Comp. and Soft. for Big Science* **8** (2024) 9.

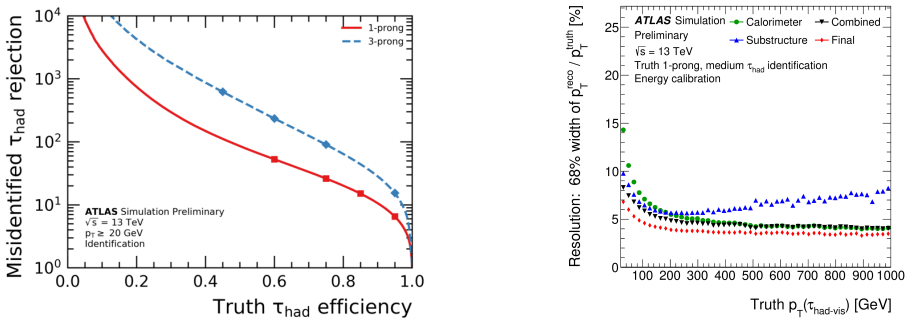

(a) (b)

Figure 6: (a) Rejection for misidentified 1-prong and 3-prong τ_{had} candidates from dijet background events as a function of the efficiency for truth τ_{had} originating from $\gamma* \rightarrow \tau\tau$ events; (b) The resolution of the calorimeter, substructure, combined and final (BRT-based) energy calibration shown for 1-prong candidates.

[4] ATLAS Collaboration, *Eur. Phys. J. C* **83** (2023) 1081.

[5] ATLAS Collaboration, ATL-PHYS-PUB-2023-023.

[6] ATLAS Collaboration, ATL-PHYS-PUB-2023-011.

[7] *CERN/SPC/1068, CERN/FC/6014, CERN/3255* (2016) .

[8] ATLAS Collaboration, IDTR-2023-05.

[9] ATLAS Collaboration, *Eur. Phys. J. C* **83** (2023) 686.

[10] ATLAS Collaboration, *JINST* **19** (2024) P02009.

[11] ATLAS Collaboration, *JHEP* **2024** (2024) 162.

[12] ATLAS Collaboration, 2402.05858.

[13] ATLAS Collaboration, *Eur. Phys. J. C* **84** (2024) 455.

[14] ATLAS Collaboration, *Eur. Phys. J. C* **83** (2023) 761.

[15] ATLAS Collaboration, *Mach. Learn.: Sci. and Technol.* **5** (2024) 035051.

[16] ATLAS Collaboration, ATL-PHYS-PUB-2022-027.

[17] ATLAS Collaboration, ATL-PHYS-PUB-2023-020.

[18] ATLAS Collaboration, ATL-PHYS-PUB-2023-021.

[19] ATLAS Collaboration, ATL-PHYS-PUB-2022-044.

[20] ATLAS Collaboration, MUON-2023-02.

[21] ATLAS Collaboration, EGAM-2022-04.

[22] ATLAS Collaboration, FTAG-2023-01.